Available online at www.sciencedirect.com

ScienceDirect

Energy Procedia 8 (2011) 672–680

Energy Procedia

SiliconPV: 17-20 April 2011, Freiburg, Germany

Effect of Al Contact Pitch on Rear Passivated Solar Cells

I.Cesar [a] *, A.A. Mewe [a], P. Manshanden [a], I.G. Romijn [a], L. Janßen[b], A.W. Weeber [a]

[a] *ECN Solar Energy, P.O. Box 1, .1755 ZG Petten, The Netherlands * email: cesar@ecn.nl*

[b] *Solland Solar Cells BV, Bohr 10, NL 6422 RL Heerlen, The Netherlands*

Abstract

In search of solar cell concepts that allow processing of thinner wafers (<150 μm), the conventional full Al rear side of p-type solar cells is replaced by an open rear metallization combined with a dielectric passivation layer. We estimate that this modification to the cell concept could result in a gain of 0.3-0.4% in absolute efficiency for a rear passivated multi-crystalline solar cell with local contacts. The gain can only be obtained when a well passivating dielectric layer is applied and Al contacts are formed with a high-quality local BSF. Three rear contacting designs are discussed: interconnected point contacts (PERC), bifacial cell with line shaped rear contacts (PASHA) and a bifacial MWT with a web pattern on both sides (ASPIRe). For these cell concepts, the performance of SiNx and Al_2O_3 as rear passivating layers are discussed in terms of local EQE measurements. A simple equivalent circuit is discussed to describe the parabolic LBIC pattern which is induced by inversion layer shunting between the rear metal contacts. The influence of the fixed charge density and the metallization pitch is discussed.

© 2011 Published by Elsevier Ltd. Selection and/or peer-review under responsibility of SiliconPV 2011.

Keywords: Multi-crystalline Silicon; P-type; Aluminum-Oxide; PECVD; Silicon-Nitride; Inversion Layer Shunt; Passivation.

1. Introduction

Dielectric layers are implemented as rear-side passivating layers in various cell concepts such as the PERC (Passivated Emitter and Rear Cell), PASHA (Passivated on all side H-pattern) but also in back contacted solar cells as MWT (Metal Wrap-Through), EWT (Emitter Wrap-Through) and IBC (Interdigitated Back Contact). These cell designs consist of metallization patterns which contact the cell's rear side while the un-contacted area is passivated with a dielectric layer. The passivation mechanism of these dielectric layers is to neutralize recombination centers at the Si wafer surface (chemical passivation) or to electro-statically repel one type of the recombining carriers from the surface (field-effect passivation) or a combination of the two passivating mechanisms. The electrostatic field is induced by

1876–6102 © 2011 Published by Elsevier Ltd. Selection and/or peer-review under responsibility of SiliconPV 2011.
doi:10.1016/j.egypro.2011.06.200

fixed charges in the dielectric layer near the Si interface which can induce an n-type inversion layer in the p-type silicon. Understanding the effect of the fixed charges in the dielectric layers on the various cell concepts is important as phenomena like inversion layer shunting (ILS) have shown to impede the cell performance severely. This phenomenon (ILS) occurs when the inversion layer is shunted by a metal contact at the rear and is studied by Dauwe et al [1] and later by Meemongkolkiat et al [2]. In absence of ILS, we have previously calculated that rear passivated multi-crystalline solar cells could show a gain of 0.3-0.4% in absolute efficiency as compared to the standard H-pattern solar cell with a full area Al-BSF on the rear [3]. In this work we present an extension to the PC1D model proposed by Dauwe et al in order to simulate these LBIC profiles and use it to illustrate the effects observed in three rear passivated cell concepts that employ SiNx (positive fixed charges) as rear passivation layer. The metallization patterns investigated for rear passivated cell designs, consist of line (PASHA) and dot (PERC) patterns as well as a web-patterned MWT cells (ASPIRe, All Sides Passivated and Integrated at the Rear). In order to illustrate the cell performance in absence of inversion layer shunting we compare LBIC mappings of two ASPIRe cells that are passivated on the rear either by a SiNx (positive fixed charges) or by an Al_2O_3 layer (negative fixed charges).

Nomenclature

R_{ILS}	Inversion layer shunt resistance [Ω].
R^{sh}_{ILS}	Sheet resistance of inversion layer [Ω/□]
x	Distance in inversion layer to metal contact [mm]
L	Laser line and contact finger length[mm]

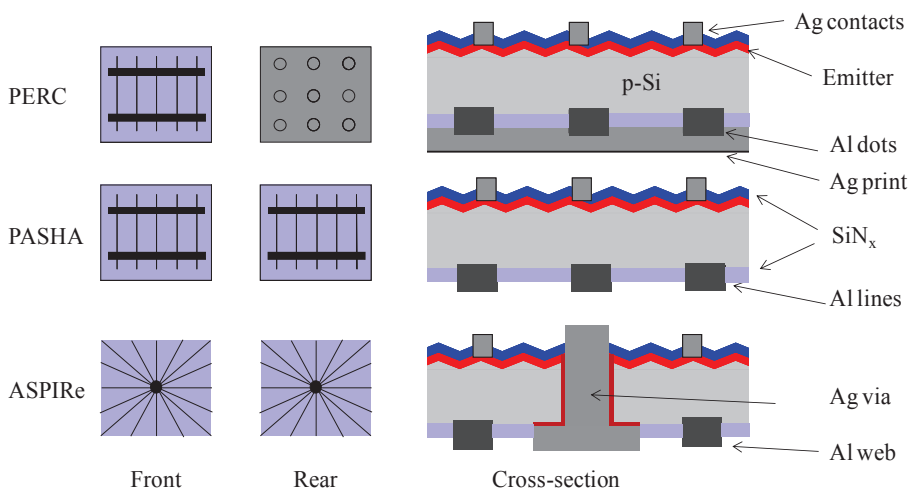

Figure 1, Rear passivated cell concepts PERC, PASHA and ASPIRe that are discussed in this work. The open areas between the rear aluminum contacts are passivated with SiNx. In the case of the PERC concept the 1 mm pitched point contacts are fired through the SiNx coating and are interconnected with a full-area silver print afterwards. The PASHA and ASPIRe (MWT) concepts consist of an H-pattern and web pattern respectively. In the case of the ASPIRe, the centre of the front web pattern of Ag contacts does not overlap with the centre of the back web pattern of Al contacts. To study passivation properties of a passivation layer without inversion layer shunting the rear SiNx layer of the ASPIRe cell is replaced by Al_2O_3.

2. LBIC profiles of investigated cell concepts

The investigated cell concepts are a p-type solar cell with H-pattern front side metallization and a p-type MWT cell, both with a rear passivation layer and open metallization patterns to contact the base. The rear

Al contacts were fired through the rear dielectric and the metallization designs consist of a dot pattern covered by metal over layer for the H-pattern cell [3] and a web pattern for the MWT cell [7] as illustrated in Fehler! Verweisquelle konnte nicht gefunden werden.. The PASHA concept with line shaped contacts is discussed in paragraph 5.

To determine the relation between Al contact pitch and the local quantum conversion efficiency between the Al contacts, p-type mc-PERC cells were prepared with 1 mm pitched contacts on a SiNx passivated rear and interconnected by a full-area silver print afterwards. In the corners on the rear of the cell, patterns were printed where the Al contact dots were omitted as illustrated in Figure 3 (these open areas represent only 0.7% of the total cell area). As the silver print does not contact the passivated base, the pitch of the Al contacts is locally increased. A typical LBIC profile that was obtained across this pattern is illustrated in Figure 2. The maximum obtained EQE increases with the distance between the contacts and saturates at a distance of about 4 mm. This 4 mm distance is much larger than can be expected from the estimated minority diffusion length of 300 µm and is a clear example of inversion layer shunting behavior which will be discussed in the next paragraphs.

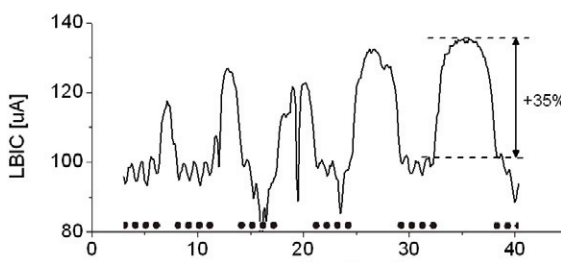

Figure 2, LBIC profile measured at 980 nm with 30% sun white bias illumination on a multi-crystalline PERC cell with a SiNx passivated rear side. Periodic minima in the profile correspond to Al rear contact positions as indicated by the dots and Figure 3.

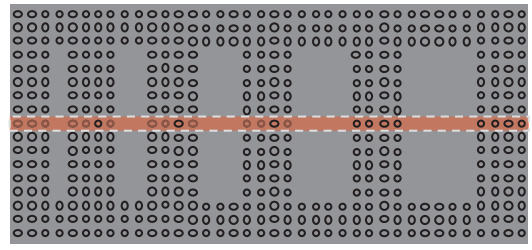

Figure 3, part of the PERC contact pattern used to analyse the contact distance effect on the LBIC signal. The red line illustrates the illumination path of the laser used in Figure 2.

Also the web shaped design of the ASPIRe cell is similarly affected by inversion layer shunting if passivated by SiNx. As the inversion layer shunt losses are dependent on the distance between Al lines it is expected that the EQE near the centre of the web structure (see Figure 1) reduces as the inversion channel length reduces and the effective shunt resistance decreases. The effect is clearly visible in **Fehler! Verweisquelle konnte nicht gefunden werden.** where the LBIC map of a SiNx passivated ASPIRe cell is compared to one that is passivated with Al_2O_3. In absence of an inversion layer, due to negative charges in the latter dielectric coating, the mapping shows a much weaker dependency on the line-to-line distance. The remaining distance effect of the EQE is caused by recombination at the Al base contacts. Here minority carriers need to diffuse to the contacts and this distance is governed by the minority carrier diffusion length which is in the case of multicrystalline wafers expected to be in the order of 300 µm. This clearly demonstrates the superiority of the Al_2O_3 coating especially for contacting patterns with small contact distances.

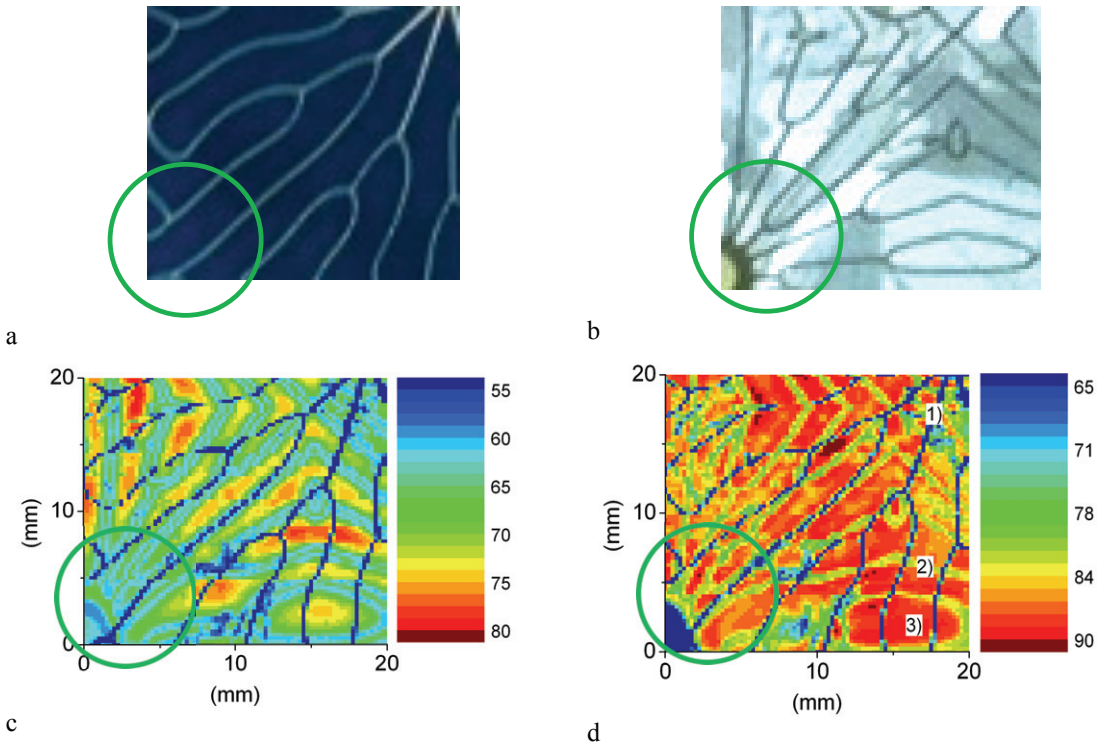

Figure 4, Design of rear passivated MWT cell (ASPIRe) showing a quarter of a unit cell of the front silver metallization spaced by a SiNx ARC (a) and the rear aluminum metallization spaced by Al_2O_3 passivated surface (b). IQE mappings measured with an LBIC setup at 980 nm with 30% sun white bias illumination of SiNx (c) and Al_2O_3 (d) passivated ASPIRe cell. The numbers in the inset correspond to 1) front metal shading as shown in (a), 2) rear metal contact as shown in (b) and 3) open passivated area. The MWT cells are made with industrial metallization design Sunweb, which is registered and owned by Solland Solar.

3. Inversion layer shunt model

Although the lifetime of double side SiNx passivated monocrystalline wafers results in surface recombination values of around 10 cm/s [4], on cell level much higher effective SRV (surface recombination velocity) values (>500 cm/s) were fitted with PC1D. Apart from the fact that additional cell processing could cause a higher effective SRV, another important reason is inversion layer shunting [1, 5, 6]. This term is often evoked in literature in correlation with floating junctions that partially contact metal leads. The floating junction in the case of SiNx layer application is formed by fixed positive charges inducing a p-n junction near the Si/SiNx interface as illustrated in Figure 5a. Through electric conduction, electrons in the n-type inversion layer can reach contacts over a much larger length scale than the diffusion length in the p-type region normally would allow. Once the inversion layer is (partially) electrically connected to the rear base metal contacts, losses up to 3.5 mA/cm^2 in J_{sc} were observed in the solar cell [1]. This current path is regarded as a shunt between the inversion layer and rear metal contacts and is referred to as inversion layer shunt (or parasitic shunt). As holds for junctions in general, if the voltage across this rear junction is small, a large fraction of the current flows through the shunt resistance. However, if the voltage increases away from the contact due to the increased current path length, the electron bands in the electron band structure flatten and the current flows across the rear junction back into the base of the cell. In this case a larger fraction of the electrons in the base is collected by the emitter

and hence the rear SRV becomes effectively lower. As a consequence the effect of the inversion layer shunt decreases as the voltage across the rear junction is increased by means of external bias potential (in darkness) and / or by bias illumination. This results in a red response that increases with increasing illumination intensity and therefore the J_{sc}-to-bias ratio is not constant but increases with increasing bias up to saturation

We present a simple equivalent circuit in combination with a PC1D model (PC1D 5.5 [8]) to describe the parabolic LBIC pattern which is induced by inversion layer shunting between two rear contact lines. The rear inversion junction is modeled in PC1D by applying positive charge (10^{12} cm^{-2}, typical for SiNx layers [1]) to the rear surface. The inversion layer shunt is modeled by a resistor which is connected to the base in parallel to the inversion layer junction as illustrated in Figure 5a and b. The inverted junction at the rear of the cell has a depth of about 100 nm. The value for the parallel shunt resistor is analytically calculated based on the geometry illustrated in Figure 5c. Here, a line shaped laser beam illuminates a rectangular area positioned in parallel to the contact finger. The width of the illuminated area corresponds to a typical laser beam width of 100 µm while the length is arbitrarily set to 10 cm. This results in a illuminated area of 0.1 cm^2 which is the cell size used in PC1D. As no bias illumination can be modeled, the laser intensity was set at 0.46 mW/cm^2 in order to be able to charge the rear junction. The intensity is compatible with standard LBIC equipment.

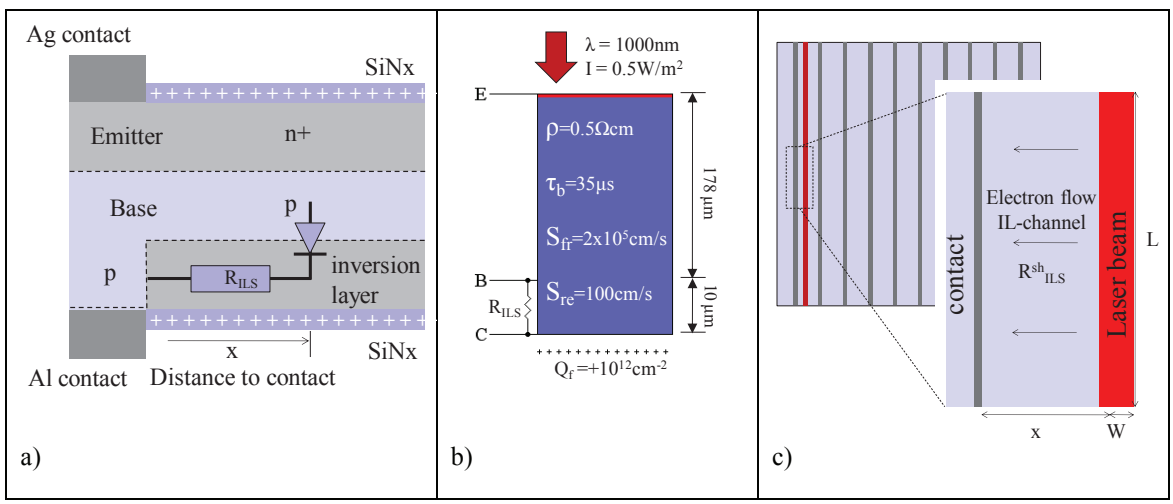

Figure 5 illustration of the model to simulate inversion layer shunting in rear passivated solar cells of the PASHA type (**Fehler! Verweisquelle konnte nicht gefunden werden.**). **(a)** cross-section of symmetry element of the PASHA cell for the case of SiNx with positive charges and rear metal contact without local BSF. The equivalent circuit represents the inversion layer junction (diode) and the inversion layer channel resistance (parallel resistor). **(b)** Cross-section of the PC1D model that simulates the solar cell including the diode and shunt resistance behavior of the rear inversion layer. The shunt resistance R_{ILS} is an input parameter which is analytically determined while the inversion layer is induced by defining a fixed positive charge density Q_f at the rear surface (10^{12} cm^{-2}). **(c)** Schematic of the rear side of a PASHA cell that illustrates the geometry that is used to analytically calculate the inversion layer shunt resistance. The contact finger and the illuminated area (laser) are separated by the inversion channel by distance x and sheet resistance R^{sh}_{ILS} (i.e. 30 kΩ/□). The illuminated area has a width W (0.01 cm) and a length L (10 cm). The symmetry element of the LBIC profile is obtained by entering R_{ILS} as function of distance x into PC1D.

As the shunt is located at the base contact, the resistance in the inversion channel increases away from the contact. The inversion layer resistance is modeled as a conductive slab as shown in Figure 5c and is calculated by:

$$R_{ILS} = \frac{R_{ILS}^{sh}\, x}{L} \qquad \text{Eq. 1}$$

Herein represent R^{SH}_{ILS} [Ω/sq] the inversion layer sheet resistance, L [cm] the length of the laser beam as well as the length of the finger and x the distance between the collection point and the shunt location at the base contact [cm].

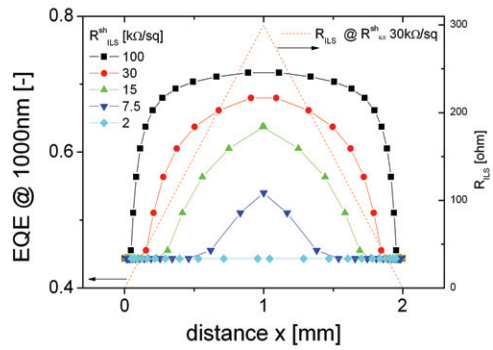

a

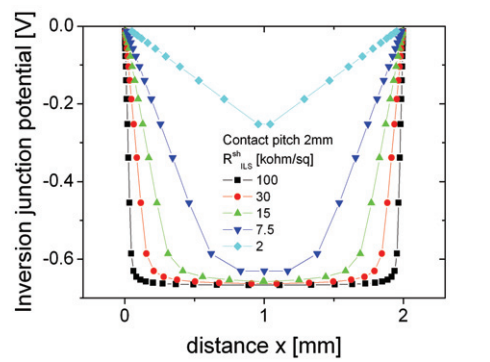

b

Figure 6, calculated LBIC profiles (a) and voltage profile across the inversion junction (voltage between contact b and c in Figure 5b.) (b) between 2 mm pitched metal rear fingers at an inversion layer resistance of 100, 30, 15, 7.5 and 2 kΩ/sq. The dashed lines illustrates the resistance in the IV channel as function of position between the contacts.

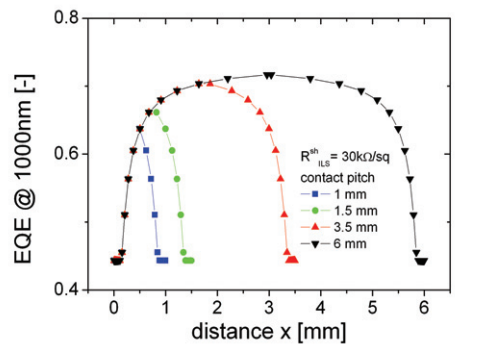

a

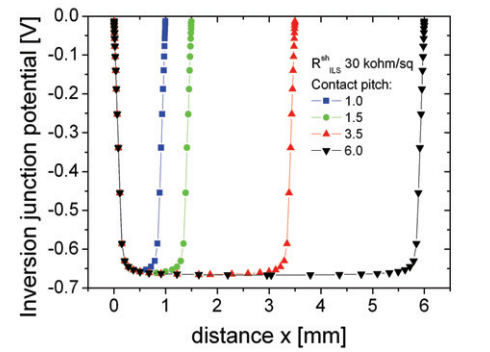

b

Figure 7, calculated LBIC profiles (a) and voltage profiles (b) across the inversion junction (voltage between contact B and C in Figure 5b.) between 1, 1.5, 3.5 and 6 mm pitched metal rear fingers at an inversion layer resistance of 30 kΩ/sq.

This approximation is considered to be valid for a rear contact grid based on parallel fingers without a local back surface field illuminated with a laser without bias light. Deviations from the measurements are expected for dot patterns and when the distance x becomes comparable to the laser width. The influence of the inversion layer shunt resistance and contact pitch on the EQE profile between the rear contacts is presented in **Fehler! Verweisquelle konnte nicht gefunden werden.** and **Fehler! Verweisquelle konnte**

cht gefunden werden. respectively. Both figures also contain the corresponding voltage profile of the rear inversion junction between the rear contacts. The voltage is negative as the inverted junction opposes the emitter junction. **Fehler! Verweisquelle konnte nicht gefunden werden.**a and b show that as the nversion channel sheet resistance increases, the EQE profiles saturate to the highest values while the rear inversion junction voltage saturates to the most negative values. Furthermore, **Fehler! Verweisquelle onnte nicht gefunden werden.** a and b illustrate that a larger contact spacing results in a higher EQE and a larger (negative) rear junction voltage. The parabolic LBIC profile for a pitch of 2 mm, becomes visible for inversion layer resistances between 100 kΩ/sq (some ILS) and 2 kΩ/sq (suffering severely from ILS). From the voltage profiles it becomes apparent that the highest EQE corresponds to the highest (negative) voltage that can build-up in the inversion junction. Towards saturation the rear junction gets charged by collection of photo-generated electrons from the base because these charges cannot leak away through the inversion layer channel to the shunt location at the metal contact. Charges that are collected close the metal contact leak easily to the shunt location as the distance and thus the resistance is small. The leak current prevents the charging of the rear junction and results locally in a low EQE and a high SRV. As charges are collected further away from the contact, the ILS resistance increases (eq. 1) which causes the leak current to decrease and the rear junction to accumulate charge. Now the rear junction becomes conductive because the bands flatten and electrons that are photo-generated in the base can flow in and out of the rear junction. The ILS resistance also increases with the ILS sheet resistance which effectively reduces the distance from the contact to the point at which the rear junction is effectively charged and the EQE value saturated. As mentioned before, the charged rear junction causes a larger fraction of the photo-generated minority carriers (electrons) to be collected by the emitter which increases mainly J_{sc}.

Dauwe et al. [1] calculated that the sheet resistance of the inversion layer channel decreased from 30 kΩ/sq to 1 kΩ/sq if the fixed charge density increased from $1x10^{12}$ cm^{-2} to $10^{13}cm^{-2}$ [1]. This was calculated in dark for a mobility of 300 cm^2/Vs and an acceptor density of 10^{16} cm^{-3}. Given typical fixed charge densities in SiNx in order of 10^{12} cm^{-2} [1], the sheet resistances used in the model presented here match very well with the values used by us (2-100 kΩ/sq). Although the range of the calculated EQE values obtained lie close to measured values for the SiNx passivated ASPIRe cell when measured without bias light (not shown here), it requires more work to determine the accuracy of the model. For this purpose other parameters that strongly influence the red response like the rear SRV, bulk lifetime and rear reflection would need to be independently determined.

However, from the model it become clear that reducing the fixed charge density increases the sheet resistance in the inversion layer. This suggests that lowering the density of fixed charges in SiNx would increase its effective SRV on cell level.

4. Conclusion

The behavior of inversion layer shunting has been experimentally demonstrated and it can be modeled with a distance dependent resistor in parallel to the rear inversion junction. This model can be implemented in PC1D to simulate the local quantum efficiency profile between two rear contacts. The sheet resistances obtained by the model for the inversion layer channel match with values reported in literature. The extend of the recombination perimeter around the poorly passivated contact can exceed the diffusion length of the minority carriers in the case of inversion layer shunting. The formation of the inversion layer is dependent on the polarity and the magnitude of both the base doping and the fixed charges in the dielectric layer. The recombination losses due to inversion layer shunting of a SiNx rear passivated solar cell, decrease when the negative fixed charge density in the dielectric layer decreases and the contact pitch increases. Inversion layer shunting can be prevented on moderately doped surfaces by

inverting the polarity of the fixed charges in the dielectric layer. This has been experimentally demonstrated by replacing the SiNx rear coating by an Al_2O_3 layer with negative fixed charge densities.

Acknowledgements

Ron Sinton is acknowledged for fruitful discussions.

Reference List

[1] S. Dauwe et al, , Low-Temperature Surface Passivation of Crystalline and its Application to the Rear Side of Solar Cells, Thesis, ISFH **2004**.

[2] V. Meemongkolkiat, DEVELOPMENT OF HIGH EFFICIENCY MONOCRYSTALLINE SI SOLAR CELLS THROUGH IMPROVED OPTICAL AND ELECTRICAL CONFINEMENT, in , Vol. Thesis, Georgia Institute of Technology **2008**.

[3] I. Cesar et al,, Parasitic shunt losses in all-side SiNx passivated mc-Si solar cells, in proceedings EU-PVSEC 2009

[4] I.G. Romijn et al,, High efficiencies on mc-Si solar cells enabled by industrial firing through rear side passivation, Proc. 21st EPVSEC, Dresden, 2006

[5] P.P. Altermatt et al, Rear surface passivation of high-efficiency silicon solar cells by a floating junction, J. Appl. Phys. 80 (6), 15, 1996

[6] K.R. McIntosh et al, A New Technique for Characterizing Floating-junction-passivated Solar Cells from their Dark IV Curves Prog. Photovolt: Res. Appl. 7, 363- 378 (1999)

[7] I.G. Romijn et al, Evaluation and assessment of the aspire concept: A new integrated mc-Si cell and module design for high efficiencies, in Proc. EU-PVSEC 2010.

[8] P. Basore and D. Clugston, PC1D Version 5.5 © 2000